



Influence of a thin aluminum hydroxide coating layer on the suspension stability and reductive reactivity of nanoscale zero-valent iron



Yi-bo Hu, Xiao-yan Li*

Environmental Engineering Research Centre, Department of Civil Engineering, The University of Hong Kong, Pokfulam, Hong Kong, China

ARTICLE INFO

Keywords:

Nanoscale zero-valent iron
Core-shell structure
Aluminum hydroxide shell
Suspension stability
Reductive reactivity

ABSTRACT

A novel structured material, aluminum hydroxide-coated nanoscale zero-valent iron (NZVI@Al(OH)_3), was synthesized to improve the applicability of NZVI in environmental remediation. Using a rate-control precipitation method, the surface of NZVI was covered with a thin shell of amorphous Al(OH)_3 . ζ -potential of NZVI under a weak alkaline condition became positive after coating with the Al(OH)_3 shell. NZVI@Al(OH)_3 performed remarkably higher suspension stability in aqueous phase than bare NZVI, owing to the increased electrostatic repulsion and the reduction of magnetic attraction between the NZVI@Al(OH)_3 particles. Results of H_2 generation test indicated that the pH buffering capacity of the Al(OH)_3 shell and the enlarged surface area benefitted the reductive reactivity of NZVI@Al(OH)_3 . Additionally, the adsorption capability of the positive Al(OH)_3 shell facilitated the reduction and detoxification of contaminants on the NZVI surface. Consequently, the core-shell structure dependent modification with a thin inorganic shell with multiple functions is a promising design for environmental nanomaterials, and the NZVI@Al(OH)_3 synthesized in this study is a feasible and environmentally benign material for environmental remediation.

1. Introduction

The high reactive surface area ($10\text{--}100 \text{ m}^2/\text{g}$) of nanoscale zero-valent iron (NZVI) makes it an attractive material for various environmental applications, including the removal of contaminants such as hexavalent chromium [1,2], arsenic [3], chlorinated aliphatics [4], or nitro-aromatics [5] from the subsurface environment. However, strong magnetic attraction between the NZVI nanoparticles causes them to agglomerate into larger clusters, or aggregates, in aqueous solution [6]. The increased size of these clusters diminishes their effective surface area, and makes it difficult for NZVI particles to migrate through water-saturated porous media for much-needed *in-situ* remediation [7]. The precipitation of iron oxidation products on the NZVI surface during application also rapidly decreases the reactivity of the NZVI [8].

To prevent the aggregation of NZVI dispersions, a wide array of polyelectrolytes have been used to stabilize NZVI in laboratory and field studies [9,10]. Adsorption of polymers on the NZVI surface can introduce a large negative charge, thereby increasing the electrostatic repulsion between particles to prevent aggregation. An improvement in colloidal stability makes more of the surface area available for chemical reactions. Another way to increase the reactivity is to dope NZVI with noble metals to form bimetallic or trimetallic nanoparticles [11,12]. Doped noble metals can accelerate electron transfer from the Fe^0 anode

to the noble metals, and thus improve the formation of atomic hydrogen for chemical reactions [11].

However, concerns have been raised over the environmental compatibility and toxicity of the polymers and noble metals involved in the NZVI synthesis and application [10]. Therefore, using environmentally benign modifications for NZVI seems to be a more attractive and practical approach. Mg-aminoclay [13], pillared bentonite [14] and porous carbon [15] can be applied to support NZVI, which can prevent the NZVI particles from aggregating and induce the mass transfer of contaminants from the solution onto the NZVI surface. Electromagnetic induction has been used to accelerate dichlorination with NZVI [16,17]. However, these approaches always require large amounts of the modification materials (several times the quantity of NZVI by weight) or sophisticated techniques, which increases the technical difficulty and the cost of NZVI modification and application.

Aluminum hydroxide (Al(OH)_3) is a safe and environmentally abundant material that has been widely used as a low-cost, environmentally friendly adsorbent [18]. Al(OH)_3 nanoparticles have their zero point of charge from around 9–11.5 [19,20], and normally they are positively charged in water or in the subsurface environment (pH 6.5–8). Therefore, negatively charged solutes such as phosphate [21], arsenate [22], or fluoride ions [23] can be effectively adsorbed and removed from the aqueous environment by Al(OH)_3 . Zhao et al.

* Corresponding author.

E-mail address: xlia@hku.hk (X.-y. Li).

(2010) used Fe_3O_4 as a magnetic core to support $\text{Al}(\text{OH})_3$ for quicker adsorption and separation of contaminants from water [23]. With a covering of non-magnetic $\text{Al}(\text{OH})_3$ on the Fe_3O_4 surface, the magnetic attraction between particles can be greatly weakened.

The surface properties and non-magnetic features of $\text{Al}(\text{OH})_3$ make it a promising material for improving the stability and chemical reactivity of NZVI. However, no techniques involving the coating of NZVI particles with such an inorganic substance have yet been reported, and the results of such coating have not been determined. In theory, the core-shell structures can be more effective than composites and/or supportive structures for modifying the surface properties and the intrinsic reactivity of the core materials [24,25]. In this study, we developed a new technique to synthesize NZVI with a thin $\text{Al}(\text{OH})_3$ coating shell, thereby forming novel $\text{Al}(\text{OH})_3$ -coated NZVI (NZVI@ $\text{Al}(\text{OH})_3$) nanoparticles. The stability of these nanoparticles in suspension was evaluated, and their reactivity was systematically studied with H_2 generation and 4-nitrophenol (4-NP) reduction. The coating of NZVI particles with a proper amount of $\text{Al}(\text{OH})_3$ was found to be highly effective for improving the suspension stability, chemical reactivity and longevity of NZVI. The core-shell structure and material properties of NZVI@ $\text{Al}(\text{OH})_3$ were also characterized to study multiple mechanisms influencing the improvements.

2. Materials and methods

2.1. Materials

FeCl_3 , NaOH ($\geq 99\%$), and HCl (37%) were obtained from VWR International; NaBH_4 (98%) and 4-NP (99%) were purchased from Acros; ethanol and methanol (ACS, ISO, Reag. Ph. Eur.) were obtained from Merck; and anhydrous AlCl_3 (99%) and NaHCO_3 (99.5%) were purchased from Sigma-Aldrich and UNI-CHEM, respectively.

2.2. Synthesis of BNZVI and NZVI@ $\text{Al}(\text{OH})_3$

Bare NZVI (BNZVI) was prepared by chemical reduction of FeCl_3 with NaBH_4 , following the borohydride reduction method described previously by others [26,27]. In brief, a 0.4 M NaBH_4 aqueous solution was added into 71.5 mL of a 0.01 M FeCl_3 aqueous solution at a rate of 4.5 mL/min as controlled by a peristaltic pump (Longer Pump BT100-2J) and then mixed with mechanical stirring. After a 10-min injection and reaction period, the BNZVI particles that formed in the solution were separated by a magnet, and washed three times with water and three times with ethanol in a nitrogen gas atmosphere. The ethanol washing was assisted with sonication (40 kHz, 100 W) to completely remove impurities.

A rate-control precipitation method was applied to coat $\text{Al}(\text{OH})_3$ onto the NZVI surface, thereby synthesizing $\text{Al}(\text{OH})_3$ -coated NZVI particles, or NZVI@ $\text{Al}(\text{OH})_3$. The coating was conducted in a 100-mL flask reactor, sealed with a cap with needles inserted for chemical injection and atmospheric control. To protect the NZVI from oxidation, the coating process was performed in an N_2 atmosphere in the flask, at room temperature ($23 \pm 1^\circ\text{C}$). First, 20 mg of BNZVI in 40 mL of ethanol was sonicated for 5 min. An ethanol solution of AlCl_3 with an Al concentration of 1 g/L was then injected into the BNZVI slurry in the flask. To bring about different thicknesses of coating, the Al dose in relation to the Fe content ($m_{\text{Al}}/m_{\text{Fe}}$) was varied from 3 to 10 wt%; this corresponded to the AlCl_3 concentration varying from 0.55 to 1.76 mM in the BNZVI slurry. Lastly, 3 mL of NaOH ethanol solution was introduced into the BNZVI slurry via a syringe pump (Longer Pump TJ-3A) at an injection rate of 1 mL/min. The overall molar ratio of OH to Al was controlled at 3. Sonication was used to keep the NZVI particles well separated during the whole coating process. Upon completion, the particles were thoroughly washed with methanol and ethanol to remove NaCl . The synthesized BNZVI and NZVI@ $\text{Al}(\text{OH})_3$ were both stored in ethanol and used within one day to prevent oxidization. The

NZVI stock suspension was washed with deoxygenated DI water or blow-dried with N_2 gas, when needed, before use. For comparative tests, particles of iron oxides and pure $\text{Al}(\text{OH})_3$ were also synthesized, following the methods described in Supporting Information (SI).

2.3. Characterizations

The morphology and structural details of the obtained BNZVI and NZVI@ $\text{Al}(\text{OH})_3$ particles were examined by using a scanning electron microscope (SEM, Hitachi S-4800 FEG) and a transmission electron microscope (TEM, FEI Tecnai G2 20 S-TWIN). The BNZVI and NZVI@ $\text{Al}(\text{OH})_3$ were further characterized by X-ray diffraction (XRD, D8 Advance diffractometer) for their crystalline features, by X-ray photoelectron spectroscopy (XPS, Physical Electronics PHI 5600) for their surface compositions, by vibrating sample magnetometer (VSM, Lake Shore 7037) for the magnetism saturation values (M_s), and by a BET surface area analyzer (Beckman Coulter SA3100) for their specific surface areas. An acid digestion was also used to determine the resulting coating mass of $\text{Al}(\text{OH})_3$ (Al/Fe , wt%) for different Al coating doses by digesting nanoparticles in a 2% HCl aqueous solution. Concentrations of dissolved Fe and Al ions were measured by an inductively coupled plasma optical emission spectrometry (ICP-OES, PerkinElmer Optima 8300). A Delsa Nano C Particle Analyzer (Beckman Coulter) was used to measure the particle size (diameter, D) distributions and ζ -potentials of both the BNZVI and NZVI@ $\text{Al}(\text{OH})_3$. NZVI particles were suspended in a 1.0 mM deoxygenated NaHCO_3 aqueous solution ($\text{pH} = 8.3 \pm 0.1$) and then sonicated for 20 s before taking the measurements.

2.4. Sedimentation test

The sedimentation test was conducted to evaluate the stability of the BNZVI and NZVI@ $\text{Al}(\text{OH})_3$ in suspension [6]. This test was conducted in a 1-cm optical cuvette, which was also used for indication of particle concentrations by UV-vis spectrophotometry (Biochrom Libra S12). Typically, a BNZVI or NZVI@ $\text{Al}(\text{OH})_3$ particles with a NZVI concentration of 0.1 g/L were suspended in a deoxygenated 1.0 mM NaHCO_3 solution. The cuvette was filled with 2 mL of the solution, so that the UV-vis light could illuminate the top region of the dispersion in the cuvette during the sedimentation test. The optical absorbance of a colloidal suspension can be well correlated with the colloidal concentration [6]. For a sedimentation test on the NZVI particles in suspension, after a 20-s sonication, the dispersion was monitored at 508 nm to record the change in its optical absorbance (I_t) over time.

2.5. Reactivity test – H_2 generation

The batch H_2 evolution test was conducted under an anaerobic condition in 126-mL serum bottles to evaluate the reactivity of NZVI with different masses of $\text{Al}(\text{OH})_3$ coating following the approach previously described [28]. Typically, a serum bottle was filled with 80 mL of deoxygenated dispersion containing 0.1 g/L NZVI and 1.0 mM NaHCO_3 . Operated in a glove box filled with pure N_2 gas, the bottle was capped with a rubber stopper and an aluminum flip-off cap, and thereby the headspace of the serum bottle was initially filled with pure N_2 . The test bottles were then placed on a shaker at room temperature ($23 \pm 1^\circ\text{C}$). A 200 rpm rate of shaking was applied to induce the reaction and perform the test. During the reaction, H^+ in water was reduced by the NZVI to produce H_2 . Gas samples of 50 μL were taken from the headspace at various time intervals to quantify the H_2 production. After the test, a deoxygenated 37% HCl aqueous solution was injected into the bottles to digest all Fe^0 . Assuming that the stoichiometry molar ratio of Fe^0 and produced H_2 is 1:1, the total H_2 production in the headspace was measured to indicate the total amount of Fe^0 involved in the reaction [29,30]. The concentration of H_2 produced in the headspace of the test vial was measured in term of the volume fraction (vol

%) by a gas chromatograph (GC9890B, Shanghai Linghua Instrument) equipped with a thermal conductivity detector.

2.6. Reactivity test – 4-NP reduction

Batch experiments were conducted on the reduction of 4-NP as a model contaminant to study the reactivity of BNZVI and NZVI@Al(OH)₃ and to investigate their potential use in decontamination under anaerobic conditions. Typically, 40 mL of a deoxygenated aqueous solution containing 0.1 g/L NZVI and 1.0 mM NaHCO₃ was poured into a 43-mL vial, which served as a reactor sealed with a PTFE septum. Stock 4-NP solution (5 g/L) was injected into the vial to produce an initial 4-NP concentration of 0.1 g/L and an initial pH of 7.3. The reactor vials were placed on an end-over-end rotator that was spun at 60 rpm at room temperature (23 ± 1 °C). One mL samples of the dispersion were taken at predetermined time intervals and filtrated through a 0.45 µm membrane. The filtrate was diluted 10 times and the pH of the diluted solution was adjusted to around 10 before the measurement of 4-NP. For chemical analysis of the solution, UV-vis spectrophotometry was used with a scanning range of 250–500 nm. An adsorption peak at 400 nm was assigned for the 4-NP, and an adsorption peak at 295 nm was assigned for the 4-aminophenol (4-AP), which was the reduction product of 4-NP [31]. The filtrate was also measured by the ICP-OES or an ICP-mass spectrometry (ICP-MS, Agilent 7900) to detect the dissolved metallic ions after the reaction. Limits of the ICP-MS detection of Fe and Al ions were 0.068 and 0.157 µg/L, respectively. The solution pH before and after the reactions was measured with a pH meter (Edge, Hanna Instrument).

2.7. Longevity test

Aerobic and anaerobic corrosion were processed, respectively, prior to the 4-NP reduction test to evaluate the longevity of BNZVI and NZVI@Al(OH)₃ under different corrosive conditions. For a typical aerobic corrosion test, a 20 mL NZVI suspension containing 0.1 g/L NZVI and 1.0 mM NaHCO₃ was placed in a sealed 23-mL bottle. The suspension was initially oxygenated to reach a dissolved oxygen (DO) concentration of around 7 mg/L, and the 3-mL headspace was filled with air. The sealed reactor was rotated at 40 rpm on a roller to effect the dynamic aerobic corrosion. The anaerobic corrosion test was conducted similarly; however, the NZVI suspension was deoxygenated and the headspace was filled with N₂ gas before corrosion. The reactor was shaken once per day to simulate a static anaerobic corrosion condition [32].

After different time periods of corrosion, the NZVI particles were retrieved with magnetic separation, and the supernatant was removed under an anaerobic condition. The reactivity of the recovered NZVI particles was then assessed with the anaerobic 4-NP reduction test. Meanwhile, the supernatant was filtrated with a 0.45 µm membrane, and the amount of leached metallic ions in the filtrate was measured by the ICP-MS.

3. Results and discussion

3.1. Characterizations

With Al doses of 3, 4, 5, and 10 wt% added into the NZVI slurry, the resulting Al(OH)₃ coating mass were found to be 0.4, 1.0, 3.4, and 8.1 wt%, respectively, for the coated NZVI@Al(OH)₃ nanoparticles (Fig. 1a). Accordingly, the Al deposition efficiency (Al_{coat}/Al_{dose}) increased from 13% to 81%. The SEM photographs indicated that BNZVI nanoparticles 50–100 nm in diameter were synthesized with smooth surfaces (Fig. S1a). After coating, the NZVI@Al(OH)₃ particles were covered with a rough coating surface (Fig. S1b).

The TEM images showed that the BNZVI particles were initially covered with a thin surface layer around 3.5 nm thick (Fig. 1b). This

layer was the iron oxide film formed by iron oxidation [33]. The particles were further coated with Al(OH)₃ to form a core-shell structure, and this shell was apparently more transparent than the Fe⁰ core or the iron oxide film. The average shell thicknesses, as measured from the TEM images, were 3.9 ± 0.6, 4.3 ± 1.3, 6.7 ± 1.4, and 13.6 ± 6.8 nm, with the coating amounts of 0.4, 1.0, 3.4, and 8.1 wt%, respectively (Fig. 1c–f). Elemental analysis profiles for the regions in the TEM images were obtained by energy dispersive X-ray spectroscopy (EDS). The EDS spectrum of the BNZVI showed peaks for Fe and O only, whereas the Fe, O, and Al peaks were obtained from the EDS spectrum of NZVI@Al(OH)₃ (Fig. S2).

During the injection of NaOH into the AlCl₃ solution for coating onto the NZVI nanoparticles, Al³⁺ ions were deprotonated and polymerized with hydroxyl binding to form polycations in cage-like structures [34]. The molecular weights of these polycations were expected to rise with increases in the OH/Al ratio, and when the OH/Al ratio increased to over 2.0, the polycations could attain a molecular weight of more than 100,000 Da [35]. The solubility of the polycations in the organic solvent decreased as their molecular weights increased [36], which induced the deposition of the polycations onto the surfaces of the colloidal particles. Therefore, in this study, the rate of deprotonation and polymerization of Al³⁺ ions would be controlled by the chemical (NaOH) injection rate. Subsequently, the Al-polycations gradually precipitated and attached to the surfaces of the NZVI particles, resulting in a rather uniform coating layer. A higher dosing concentration of Al³⁺ ions increased the ratio of insoluble to soluble polycations in the solution, which led to higher efficiency in Al deposition and a thicker coating shell, as shown in Fig. 1.

The XPS spectra shown in Fig. 2 revealed the surface compositions of the BNZVI and NZVI@Al(OH)₃. The binding energies of the spectra were calibrated by the C 1 s peak at 284.8 eV. The XPS survey on the 1.0 wt% NZVI@Al(OH)₃ on Fe 2p showed surface species similar to those on the BNZVI. The deconvolution of the XPS spectrum between 704 and 730 eV indicated that various iron species coexisted on the surface in the forms of Fe⁰, Fe(II), and Fe(III) (Fig. 2a). The binding energies, the full width at half maximum (FWHM) and the percentage of the Lorentzian-Gaussian ratio (%L-G) used for the curve fittings [37–39] are shown in Table S1. The areas calculated for the peaks indicated the relative abundance for the different iron species, as summarized in Table S2. Due to the thin XPS detection depth of around only 5 nm [40], only 11.8% Fe⁰ was detected for the BNZVI, and this amount decreased to 7.9% with the Al(OH)₃ shell. The atomic concentration of iron on the surface decreased from 29.3% to 19.9% after the Al(OH)₃ coating (Table S3), which indicated the coverage of NZVI particles by the Al(OH)₃ shell.

The XPS O 1s spectrum of BNZVI could be fitted by two peaks centered at 529.6 and 531.0 eV. These two peaks could be assigned to O in the metal oxide structure (O-M), and O in the hydroxyl group bound with metal structure (OH-M), respectively (Fig. 2b). Although the binding energies of the O 1s species reported from different studies were not exactly equal, the shift around 1.4 eV between O-M and OH-M for iron (hydr)oxides has also been found by other researchers [27,38,41]. In this study, the shift of binding energy between the two O species was 1.7 eV (from 529.7 to 531.4 eV), with the FWHM increasing from 1.7 to 1.97 for NZVI@Al(OH)₃. In addition, the ratio of hydroxyl O to total O increased from 53.2% to 72.7% after coating with a 1.0 wt% Al(OH)₃ shell. These changes might have been due to the OH group bound with Al (OH-Al, centered at 531.8 eV [42]), which formed on the surface. The valence of Al was also confirmed by XPS analysis (Fig. 2c). Compared with the BNZVI, a clear peak was identified, centered at 74.2 eV, which could be assigned to Al(III) [42].

The XRD pattern of the BNZVI synthesized in this study was dominated by a broad, weak peak of iron (Fig. S3), which fit the pattern of previous results regarding the weak crystallization nature of NZVI as synthesized by the borohydride reduction method [27]. This XRD pattern of NZVI did not change after the surface coating. Additionally, the

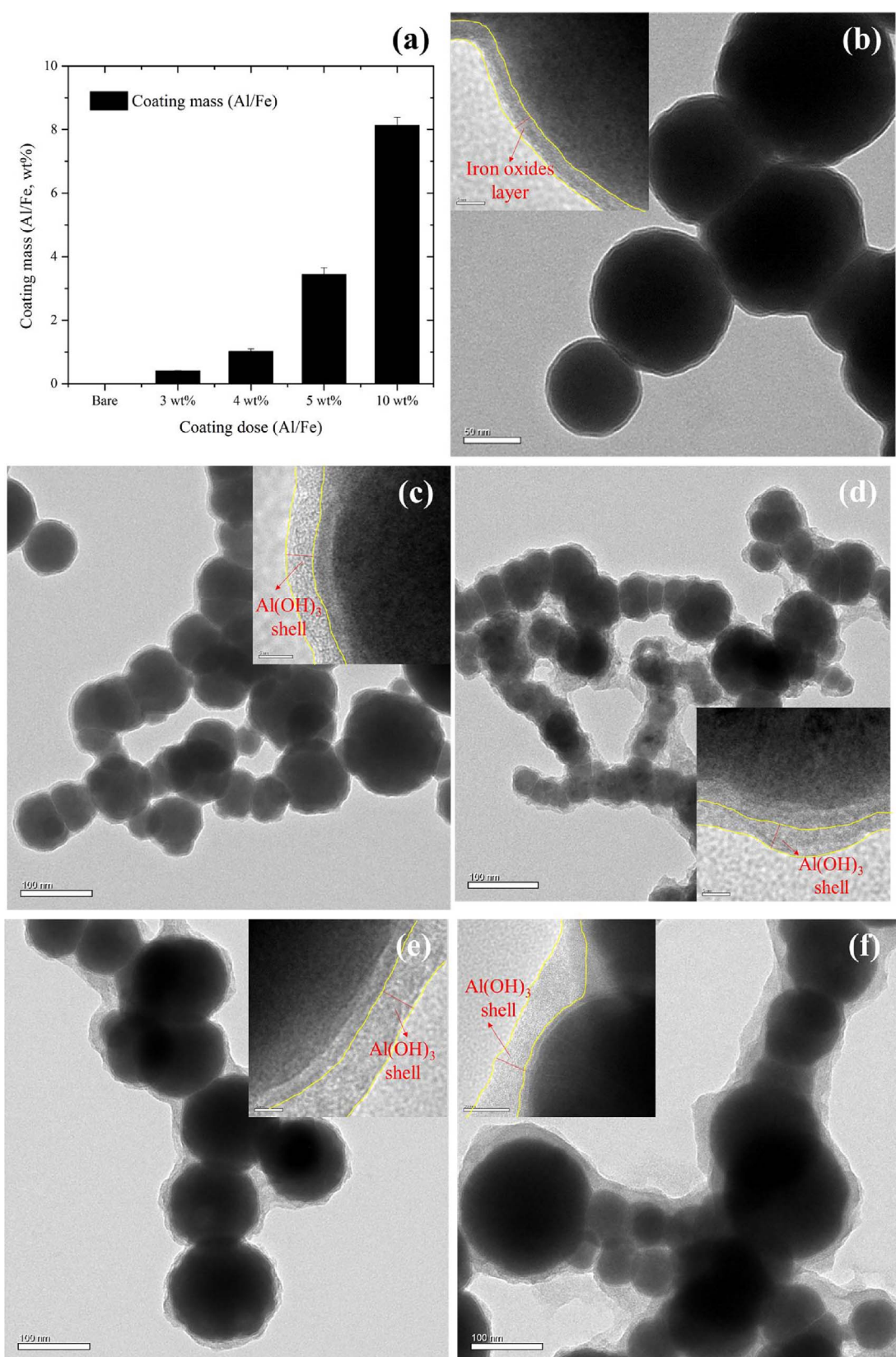


Fig. 1. (a) Al/Fe coating masses of NZVI@Al(OH)₃ with different coating does. (b) TEM images of BNZVI and (c) NZVI@Al(OH)₃ with a coating mass of 0.4 wt%, (d) of 1.0 wt%, (e) of 3.4 wt%, and (f) of 8.1 wt%.

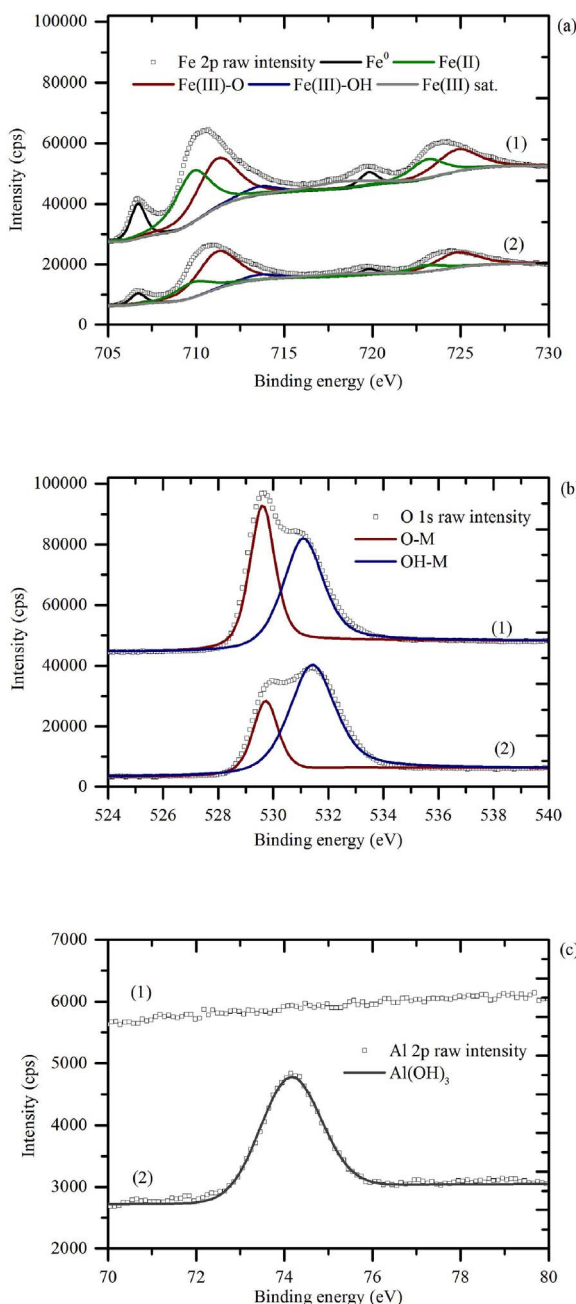


Fig. 2. XPS spectra and deconvolution spectra of (a) Fe 2p, (b) O 1s, and (c) Al 2p of (1) BNZVI and (2) 1.0 wt% NZVI@Al(OH)₃.

XRD analysis of NZVI@Al(OH)₃ and pure Al(OH)₃ synthesized at room temperature revealed an amorphous feature of Al(OH)₃ (Fig. S3). This amorphous nature of the Al(OH)₃ shell could leave defects in the shell layer that allowed solutes in the solution to transport through the shell and react with the NZVI core.

3.2. Suspension stability of NZVI@Al(OH)₃

Sedimentation curves were obtained by plotting the normalized absorbance (I_t/I_0) as a function of time (Fig. 3a). The I_0 in the suspension containing 0.1 g/L NZVI was measured as 1.2 ± 0.15 for BNZVI and for all forms of synthesized NZVI@Al(OH)₃. The decrease of I_t/I_0 indicated the decline of particle concentrations, driven by sedimentation from the top region. The sedimentation test results clearly showed that coating NZVI with Al(OH)₃ could greatly improve the particle stability and hence prevent the aggregation of NZVI and its

sedimentation in suspension. The half time of particle sedimentation (t_{half} for $I_t/I_0 = 0.5$) increased from 10.6 to 51.6 min as the Al/Fe increased from 0 to 3.4 wt%. Compared to the use of polyelectrolytes for NZVI stabilization [43] and of porous materials for supporting NZVI [13,44], the suspension stability of the coated NZVI@Al(OH)₃ increased more significantly (Table S4). Besides, a much less dosing chemicals were used for the improved NZVI stability in suspension.

The sedimentation curves of BNZVI and NZVI@Al(OH)₃ followed the pattern reported for the sedimentation of nanoparticles [6]. Before an apparently critical time (t_{crit}), the NZVI particles aggregated and settled slowly (portion I). However, when the NZVI clusters linked together to form chains and aggregates of a certain size, e.g., at t_{crit} , the NZVI particles began to settle at a much faster velocity (portion II). The two portions of the sedimentation curves were fitted by Eq. (1), to describe the removal of particles by sedimentation from the detection region:

$$\frac{I_t}{I_0} = e^{-t/\tau} \quad (1)$$

where τ is the characteristic time. For portion I of the sedimentation curve, the τ_1 of 3.4 wt% NZVI@Al(OH)₃ was 539.4, which was 8.7 times longer than the τ_1 of BNZVI (Table S5). However, the τ_2 for portion II increased by only 1.2 times with the 3.4 wt% coating mass. The comparison of τ results suggested that the Al(OH)₃ coating shell affected the stability and sedimentation of NZVI mainly by changing the rate of particle aggregation before t_{crit} . The coated NZVI@Al(OH)₃ was more stable in solution than the BNZVI, and much slower to form particle clusters and aggregations (prolonged portion I). The shape of the sedimentation curves observed in this study is different from that of the NZVI particles stabilized with supporting materials or polymers, which was often reported to exhibit a first-order decay type of sedimentation [13,43]. The sedimentation curves reported would have a relatively short portion I, without a clear turning point to indicate the critical time. The suspension stability of the reported NZVI particles was improved mainly due to the prolonged period of portion II (i.e., slow sedimentation), as portion II was extended by the stabilizers dosed. For the coated NZVI@Al(OH)₃, the Al(OH)₃ coating shell stabilized the NZVI particles, decreased the particle aggregation rate and hence extended the aggregation period, i.e. portion I of the sedimentation curve.

As previously known, several factors such as the surface charge, magnetic attraction, and collision frequency can affect the stability of NZVI particles in suspension [6,45]. To investigate the improvement in stability of NZVI with the Al(OH)₃ coating, the ζ -potential, the M_s values, and the initial sizes of the particles were measured. The BNZVI particles were negatively charged on the surface due to the iron oxide shells, with a ζ -potential of -9.7 (Fig. 3b) under the pH condition of 8.3 ± 0.1 . In contrast, the protonation of Al(OH)₃ (-AlOH_2^+) gave the NZVI@Al(OH)₃ a positively charged surface at the same pH [46], and the ζ -potential of the NZVI@Al(OH)₃ increased from $+13.3$ to $+22.2$ as the amount of Al(OH)₃ shell increased from 0.4% to 8.1 wt%. A higher ζ -potential value implied a stronger electrostatic repulsion between particles, with greater resistance to aggregation [6]. On the other hand, particle aggregation was strongly promoted by the magnetic attraction of NZVI [47]. The M_s value of NZVI@Al(OH)₃ decreased from 105.1 to 90.9 emu/g with the coating mass increase to 8.1 wt% (Fig. 3c). Hence, the improved stability of the NZVI@Al(OH)₃ particles in suspension was mainly caused by the higher electrostatic repulsion between the particles and partly by their reduced level of magnetic attraction.

However, the suspension stability of NZVI@Al(OH)₃ did not increase as the Al(OH)₃ coating mass was further increased from 3.4 to 8.1 wt%. This result could have been caused by the increased size of the NZVI particles. With an increasing Al dose, the coating shell would be thickened, increasing the size of the coated NZVI@Al(OH)₃ particles. As the Al(OH)₃ coating mass increased from 0 to 8.1 wt%, the initial particle diameter after sonication increased from 282.7 to 727.7 nm

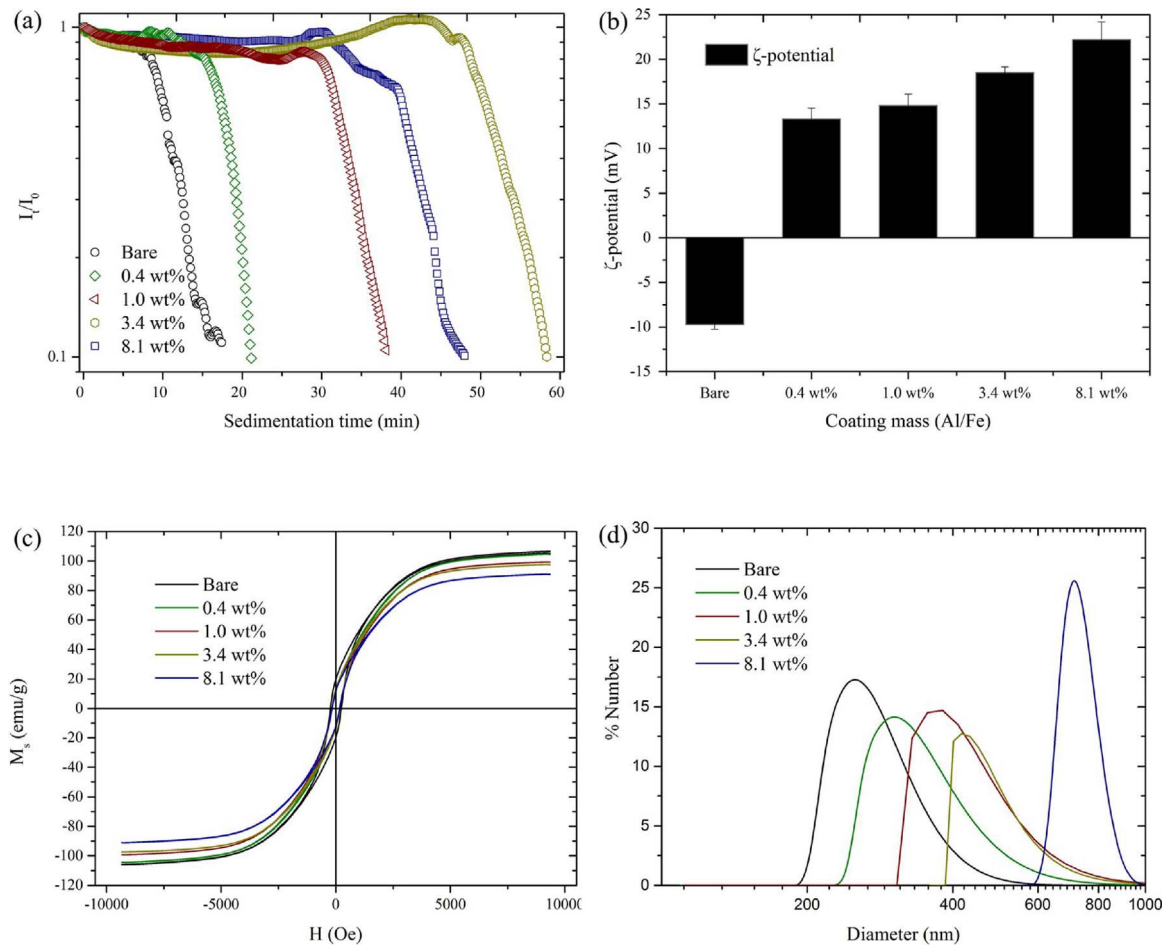


Fig. 3. (a) Sedimentation curves, (b) ζ -potential, (c) magnetic field dependent magnetization and (d) size distribution of BNZVI and NZVI@Al(OH)₃ with different coating masses (Sedimentation conditions: [NZVI] = 0.1 g/L, [NaHCO₃] = 1.0 mM, pH = 8.3 ± 0.1, T = 23 ± 1 °C).

(Fig. 3d). In accordance with the particle aggregation kinetics, such an increase in particle diameter would enhance the frequency of orthokinetic collisions between the particles [45]. Moreover, larger particles should need less time to form critical-sized aggregates. As a result, 8.1 wt% NZVI@Al(OH)₃ showed a relatively lower suspension stability than 3.4 wt% NZVI@Al(OH)₃.

The separated and suspended NZVI@Al(OH)₃ particles could be applied for various environmental applications, including injection for soil and groundwater remediation. The photographs of the suspensions after the sedimentation test (Fig. S4) indicated that the NZVI@Al(OH)₃ particles were still suspended, but the BNZVI particles had settled completely. NZVI@Al(OH)₃ particles could also be dosed in reactors for removal of pollutants from wastewater. After the treatment use in a suspension, the modified NZVI particles can be readily recovered from the treated wastewater by magnetic separation (Fig. S4c).

3.3. H₂ generation with NZVI@Al(OH)₃

The generation of H₂ from water by NZVI under an anaerobic condition indicates the chemical reactivity of the NZVI particles. The results of H₂ generation in 10 d by NZVI and NZVI@Al(OH)₃, normalized with the amounts of Fe⁰, are presented in Fig. 4a. In general, the rates of H₂ generation can be fitted with a pseudo zero-order kinetics as follows:

$$\frac{d[H_2]}{dt} = k_{obs,H_2} = k_{sa,H_2} \cdot [S] \cdot [SA] \quad (2)$$

where [H₂] is the molar ratio of the H₂ production to the amount of total Fe⁰ involved in the reaction after time t (d), k_{obs,H₂} is the observed rate

constant of H₂ generation (/d), k_{sa,H₂} is the surface area normalized rate constant of H₂ generation (L/m² d), [S] is the solid concentration of the BNZVI or NZVI@Al(OH)₃ (g/L), and [SA] is the BET surface area of the nanoparticles (m²/g). The pseudo zeroth-order pattern was also observed in previous studies for a long period of H₂ generation with a sufficient amount of residual NZVI [48–50]. It is apparent that the H₂ generation rate was independent of the amount of NZVI under the alkaline conditions, provided sufficient NZVI in the suspension. This might be due to that H₂ generation by NZVI particles was mainly a mass transport-limiting process other than a reaction-limiting process. For a sufficient amount of NZVI particles, the rate of H₂ generation was mainly controlled by the transport of H⁺ ions to the Fe⁰ surface of NZVI for reduction. As a result, the H₂ generation rate fitted well with the pseudo zero-order kinetics for a long period of the test. The BNZVI had a k_{obs,H₂} value of 0.0422 ± 0.0024/d, and a coating of NZVI with Al(OH)₃ was found to affect the H₂ generation rate. The k_{obs,H₂} increased to 0.0751 ± 0.0016/d for NZVI@Al(OH)₃ with an Al(OH)₃ coating of 3.4 wt% (Table S6). As the coating mass was further increased to 8.1 wt%, the k_{obs,H₂} somewhat decreased to 0.0569 ± 0.0035/d.

The enhancement on the observed H₂ generation rate by the Al(OH)₃ coating on NZVI was due to the increased reactive surface area. With a coating of Al(OH)₃, the BET surface area of NZVI@Al(OH)₃ increased, e.g., from 17.0 to 37.8 m²/g as the coating mass from 0 to 8.1 wt% (Fig. 4b). This was probably caused by the formation of the Al(OH)₃ shell, which hindered the particles from clustering and aggregating after sonication. However, the k_{sa,H₂} decreased gradually from 0.0247 ± 0.0014 to 0.0110 ± 0.0007 L/m² d with the increased coating masses (Fig. 4b). The results indicated that the Al(OH)₃ shell

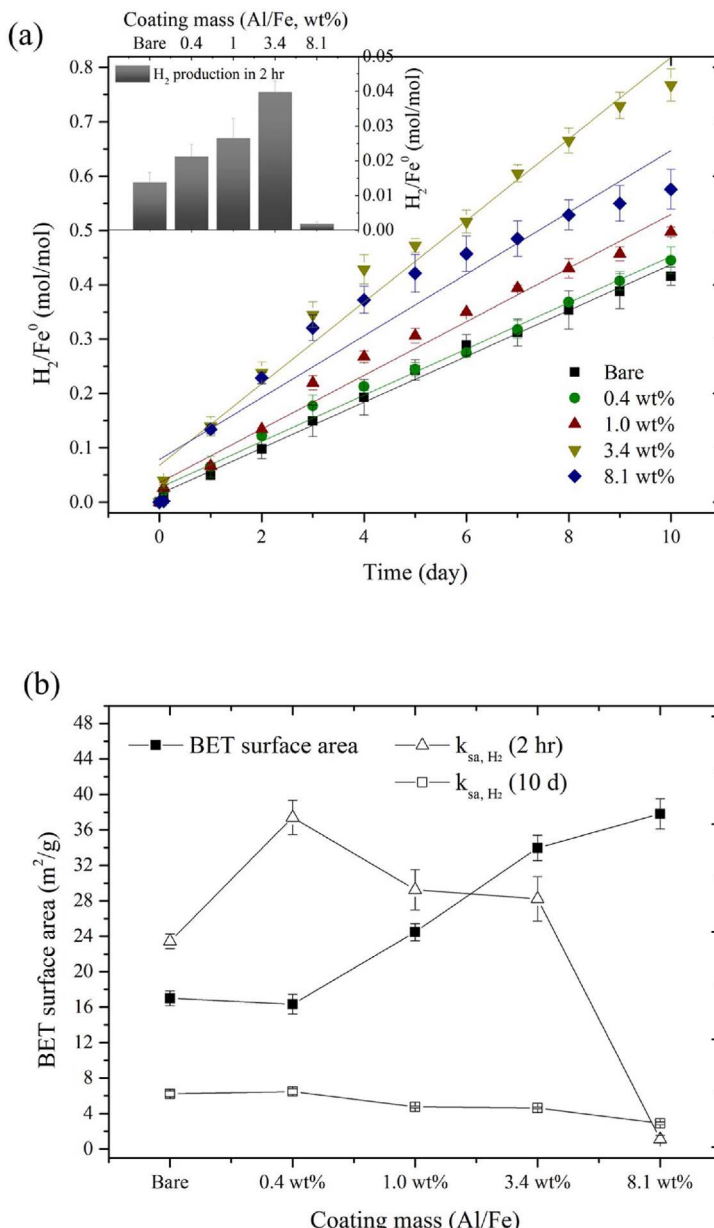
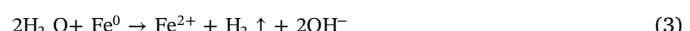


Fig. 4. (a) Anaerobic H_2 production profiles, (b) BET surface area and surface-area normalized pseudo zeroth-order rate constant ($k_{\text{sa}, \text{H}_2}$) of the H_2 production in 2 h and 10 d of BNZVI and NZVI@ Al(OH)_3 with different coating masses. The insert in (a) is the H_2 production in the first 2 h (reaction conditions: $[\text{NZVI}] = 0.1 \text{ g/L}$, $[\text{NaHCO}_3] = 1.0 \text{ mM}$, $\text{pH} = 8.3 \pm 0.1$, $T = 23 \pm 1^\circ\text{C}$).

could inhibit the mass transfer of H^+ ions to the surface of the NZVI core and decrease the anaerobic corrosion rate of Fe^0 in aqueous solutions.

It is noted that the $k_{\text{sa}, \text{H}_2}$ of NZVI with coating masses from 0 to 3.4 wt% in the first 2 h were higher than in the rest of reaction period (Fig. 4b). This phenomenon was probably due to the iron oxides produced during H_2 evolution tended to accumulate and precipitate on the NZVI surface (Eqs. (3) and (4)), resulting in a loss of accessibility and reactivity of the NZVI for chemical reactions. On the other hand, the $k_{\text{sa}, \text{H}_2}$ for the first 2 h of NZVI@ Al(OH)_3 with coating masses from 0.4 to 3.4 wt% were not lower than that of BNZVI, which trend is different with the $k_{\text{sa}, \text{H}_2}$ for 10 d. The improvements on H_2 generation of NZVI@ Al(OH)_3 in the first 2 h may be contributed by the pH buffering ability of the Al(OH)_3 shell. The Al(OH)_3 nanoparticles synthesized in this study were found to have a high pH-buffer capacity in aqueous solution (Fig. S5a), which have resulted from the protons released from the aluminol groups of Al(OH)_3 [46]. An Al(OH)_3 suspension with a concentration of 0.025 M had an average buffer capacity of 2.3 mM/pH (Fig. S5b). This buffer capacity of Al(OH)_3 tended to minimize the potential increase of pH in the vicinity of the NZVI surface, thereby

supplying more protons to Fe^0 for H_2 production [14]. In addition, the neutralization of OH^- by protons released from Al(OH)_3 could make the conditions less favorable for iron precipitation at the NZVI surface, and thereby help to sustain the particles in a state of higher reactivity. However, as the $k_{\text{sa}, \text{H}_2}$ for 10 d were not benefited by the increasing Al(OH)_3 shell, the pH buffer capacity might be insufficient and only influenced a limited portion of the NZVI reactivity.



Excessive Al(OH)_3 coating mass could reduce the reactivity of the NZVI, as was indicated by the results of H_2 generation with 8.1 wt% NZVI@ Al(OH)_3 (Fig. 4a & b). In particular, the $k_{\text{sa}, \text{H}_2}$ of 8.1 wt% NZVI@ Al(OH)_3 in the first 2 h was far lower than that of the other NZVI particles. The slower H_2 generation rate for 8.1 wt% NZVI@ Al(OH)_3 in the first 2 h suggested that the protons and produced H_2 took a longer time to pass through the thicker Al(OH)_3 shells than was the case with 3.4 wt% NZVI@ Al(OH)_3 . Overall, the results of H_2 generation confirmed the indispensable effects of the increased BET surface area and

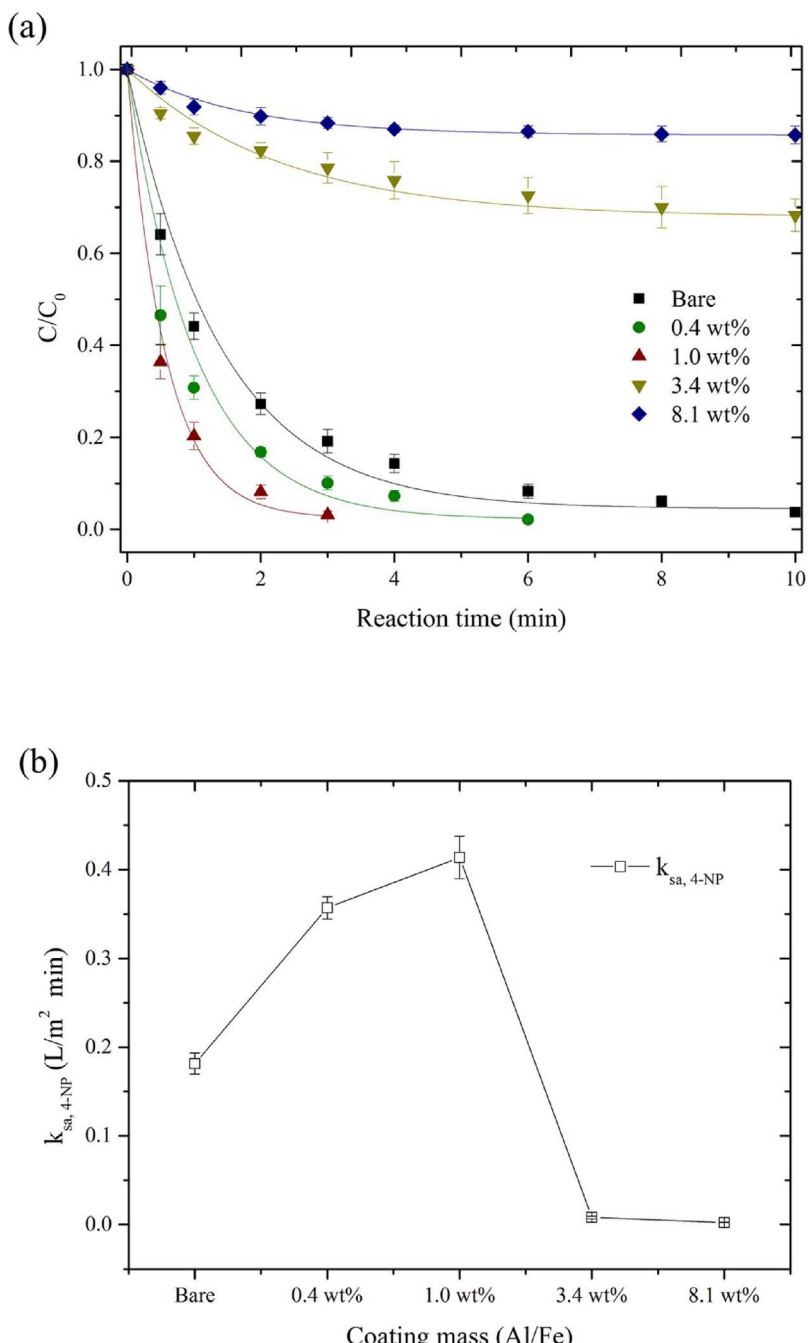
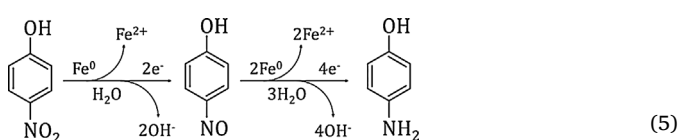


Fig. 5. (a) Anaerobic 4-nitrophenol (4-NP) reduction profiles and (b) surface-area normalized pseudo first-order rate constant ($k_{sa,4-NP}$) of the 4-NP reduction of BNZVI and NZVI@Al(OH)₃ with different coating masses (reaction conditions: [NZVI] = 0.1 g/L, [NaHCO₃] = 1.0 mM, [4-NP] = 0.1 g/L, pH = 7.3 ± 0.1, T = 23 ± 1 °C).

the buffer capacity and thickness of the Al(OH)₃ shell on the reactivity of NZVI@Al(OH)₃ particles.

3.4. 4-NP removal by NZVI@Al(OH)₃

To identify potential environmental applications, the reactivity levels of the NZVI particles with various Al(OH)₃ coatings were also tested on the reduction of 4-NP. Under an anaerobic condition, the dominant pathway of 4-NP reduction by NZVI may be described as follows:



4-NP would be firstly reduced to 4-nitrosophenol [51], which was then reduced rapidly to 4-AP [52,53]. With the formation of 4-AP, an adsorption peak can be identified at around 295 nm of the UV-vis spectrum [31,54]. The rising peak of 4-AP coupled with the declining adsorption peak of 4-NP at 400 nm evidenced the transformation of 4-NP to 4-AP in the NZVI suspension (Fig. S6a). The absorbance peaks at about 295 nm of the filtrates after complete 4-NP reduction by BNZVI and NZVI@Al(OH)₃ were similar (Fig. S6b). In the absence of the Al(OH)₃ coating shell, the BNZVI reduced 0.1 g/L of 4-NP by 96.3% after 10 min (Fig. 5a). In comparison, a reduction of 96.8% was obtained within 3 min by applying 1.0 wt% NZVI@Al(OH)₃. The rate of 4-NP reduction by NZVI can be fitted with a pseudo first-order kinetics as follows:

$$\frac{d[4\text{-NP}]}{dt} = -k_{obs,4\text{-NP}} \cdot [4\text{-NP}] = -k_{sa,4\text{-NP}} \cdot [4\text{-NP}] \cdot [S] \cdot [SA] \quad (6)$$

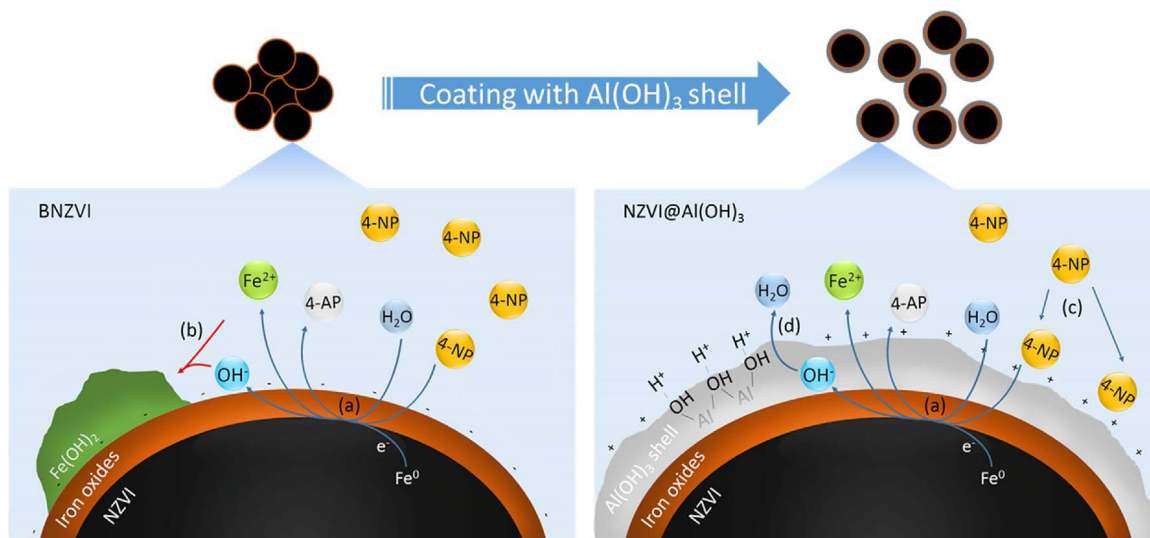


Fig. 6. Illustration for the main effects of the Al(OH)₃ coating layer on NZVI reactivity: (a) reduction of 4-NP by reactive NZVI surface, (b) adsorption and precipitation of ferrous ions on the surface of iron oxides, and (c) adsorption of 4-NP on the Al(OH)₃ surface, and (d) neutralization of the produced hydroxide ions by aluminol groups on the Al(OH)₃ surface.

where [4-NP] is the concentration (g/L) of 4-NP after time t (min), $k_{\text{obs},4\text{-NP}}$ is the observed rate constant of the 4-NP reduction (/min), $k_{\text{sa},4\text{-NP}}$ is the surface area normalized rate constant of the 4-NP reduction ($\text{L}/\text{m}^2 \text{ min}$). The Al(OH)₃ shell could increase both $k_{\text{obs},4\text{-NP}}$ and $k_{\text{sa},4\text{-NP}}$ with a proper coating ratio. (Table S7 & Fig. 5b). The BNZVI particles had a $k_{\text{sa},4\text{-NP}}$ value of $0.181 \pm 0.012 \text{ L}/\text{m}^2 \text{ min}$. Coating the NZVI with Al(OH)₃ at 1.0 wt% caused the $k_{\text{sa},4\text{-NP}}$ to increase up to $0.413 \pm 0.024 \text{ L}/\text{m}^2 \text{ min}$. However, further increases in the coating mass to above 3.4 wt% increased the mass transfer limitation for 4-NP through the Al(OH)₃ shell and lowered the $k_{\text{sa},4\text{-NP}}$ to below $0.008 \pm 0.001 \text{ L}/\text{m}^2 \text{ min}$. The trend of the change of $k_{\text{sa},4\text{-NP}}$ with the Al(OH)₃ coating mass is different from that of the k_{sa,H_2} . In addition to the increased suspension stability and NZVI reduction for H₂ generation, other factors might facilitate the 4-NP reduction. Fig. 6 gives the schematic mechanisms that intuitively compare the removal of chemical contaminants by BZNVI and by NZVI@Al(OH)₃.

For organic contaminants, they could be adsorbed onto the (hydr)oxide surface and transfer across the (hydr)oxide shell to the reactive NZVI core [55]. Thus, as illustrated in Fig. 6c, the adsorption property of the particle surfaces should be an importance factor for the surface-mediated reactivity. The adsorption of 4-NP onto the surfaces of BZNVI and NZVI@Al(OH)₃ was characterized through adsorption tests with iron oxides and pure Al(OH)₃ nanoparticles, and the adsorption behavior was described by the Langmuir isotherm (Fig. S7). Iron oxides composed of lepidocrocite and magnetite (Fig. S3) had a 4-NP adsorption capacity of $0.062 \text{ mg}/\text{m}^2$, but the value for Al(OH)₃ was $0.423 \text{ mg}/\text{m}^2$ (Table S8). The adsorption of 4-NP could be enhanced by the electrostatic interaction between the $-\text{NO}_2$ groups and the hydroxide surface via substitution of the $-\text{OH}$ groups of the Al(OH)₃ shell [56]. Hence, the Al(OH)₃ surface of NZVI@Al(OH)₃ was more favorable than the iron oxides surface of BZNVI for the adsorption of 4-NP (Fig. 6c). As a result, stronger adsorption induced the concentration of 4-NP on the NZVI@Al(OH)₃ surface, thereby contributing to its improved mass transfer and reactivity. The adsorption of 4-NP was also reported for the porous material-supported NZVI [5,57], which accelerated 4-NP reduction. However, for such a means of NZVI modification, a weight ratio of 5 between the supporting materials to NZVI was needed to have a 3-time increase in $k_{\text{obs},4\text{-NP}}$ under a neutral pH condition (Table S4) [57]. The chemical dose was massive compared to the Al(OH)₃ coating, and many of the potential adsorption sites of the supporting materials were actually far away from the NZVI surface for 4-NP reduction.

The surface compositions of BZNVI and NZVI@Al(OH)₃

nanoparticles after their reactions with 4-NP were also analyzed by the XPS technique. The elemental quantification showed that the atomic concentration of Fe on the surface of NZVI@Al(OH)₃ increased from 19.9% to 28.6% after the reaction, which was close to the result for BZNVI (30.8%). In addition, the atomic concentration of Al decreased from 5.43% to 0.70% (Table S3). Thus, the Al(OH)₃ shell were apparently covered with iron (hydro)oxides after the reaction. According to the ICP-MS results, no dissolved Al ions were detected in the filtrate, while dissolved Fe ions were detected with a concentration up to 2.7 mg/L after the complete 4-NP reduction by BZNVI and NZVI@Al(OH)₃ of 1.0 wt% (Table S9). The XPS profiles and ICP-MS results suggest that the produced Fe ions might have migrated through the Al(OH)₃ shell to precipitate onto the Al(OH)₃ surface or dissolve in the solution after the reaction. In the vicinity of NZVI@Al(OH)₃ surfaces, the OH⁻ produced from the 4-NP reduction by NZVI (Eq. (5)) could be consumed by protons released from Al(OH)₃, which would tend to limit the increase of pH and the resulting Fe(OH)₂ precipitation during the reaction (Fig. 6d). According to the pH measurements (Fig. S8), Al(OH)₃ nanoparticles served as a weak buffer, and were able to maintain the solution at a relatively lower pH level. Moreover, the negatively charged iron oxides were more favorable to the adsorption and precipitation of Fe²⁺ ions during the reaction, which covered the surface and reduced the reactivity of BZNVI (Fig. 6b).

3.5. Longevity and long-term reactivity of NZVI@Al(OH)₃

As the aqueous corrosion limits the longevity and applicability of NZVI for full-scale environmental applications [58], modifications have been made to reduce the corrosion and extend the longevity of NZVI particles [2,5,59]. In the present study, the effect of the Al(OH)₃ coating shell on the longevity of NZVI was investigated under both aerobic and anaerobic corrosion conditions. Under the aerobic condition, BZNVI particles were quickly oxidized and the suspension turned to yellow after 5 min of aerobic corrosion (Fig. S9a). After 15-min, the BZNVI particles became brownish in the suspension. As shown by the following 4-NP reduction tests, the reactivity of BZNVI decreased clearly with the time of aerobic corrosion (Fig. S10a), and the 4-NP removal efficiency decreased significantly from 96.3% to 15.9% (Fig. 7). On the contrary, the Al(OH)₃ coating shell could effectively hinder aerobic corrosion of NZVI particles (Fig. S10b). The suspension of NZVI@Al(OH)₃ at 1.0 wt% during the aerobic corrosion test appeared much less yellow than the BZNVI suspension (Fig. S9b). The 4-NP removal efficiency with the corroded NZVI@Al(OH)₃ decreased to 44.0% of the

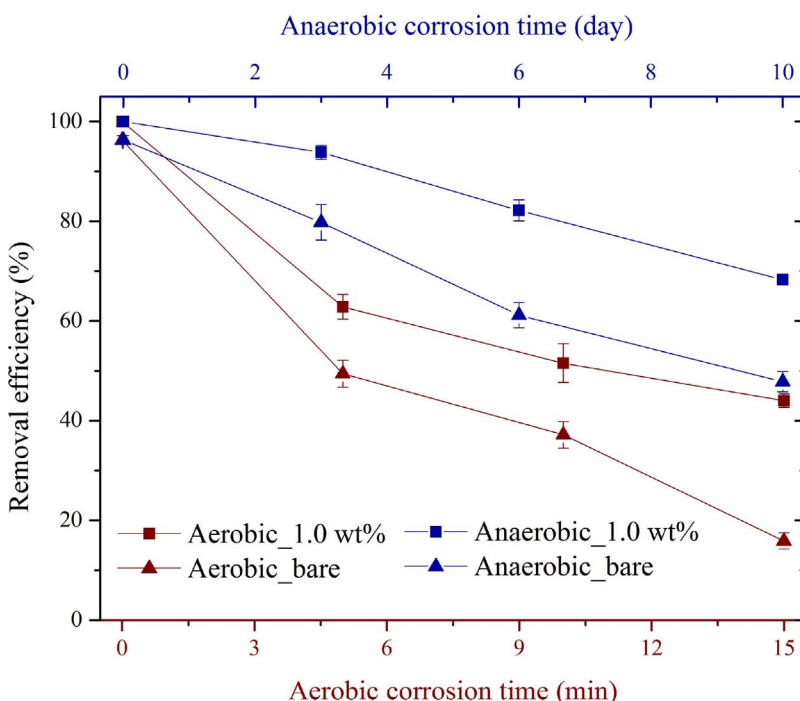


Fig. 7. The efficiency of 4-NP removal by BNZVI and NZVI@Al(OH)₃ of 1.0 wt% coating mass before and after the aerobic and anaerobic corrosion (corrosion conditions: [NZVI] = 0.1 g/L, [NaHCO₃] = 1.0 mM, pH = 8.3 ± 0.1, T = 23 ± 1 °C).

original level (Fig. 7), which was considerably higher than that with the corroded BNZVI.

The Al(OH)₃ coating shell was also able to protect the reactivity of NZVI particles under an anaerobic condition. The appearance of the BNZVI and NZVI@Al(OH)₃ suspensions did not show obvious change after 10 day of corrosion in the anaerobic environment (Fig. S11). However, the removal efficiency of 4-NP with BNZVI decreased to 47.8% after the anaerobic corrosion (Fig. 7). In comparison, the 4-NP removal efficiency with NZVI@Al(OH)₃ after the anaerobic corrosion only decreased to 68.2%.

The extended longevity of NZVI@Al(OH)₃ is likely due to the shield effects provided by the Al(OH)₃ coating shell on the NZVI surface. As indicated by the results of H₂ generation, the surface of NZVI@Al(OH)₃ was less accessible and hence less vulnerable than that of BNZVI when exposed to competitive oxidants, such as H⁺ ions and DO. Furthermore, the iron corrosion produced Fe²⁺ (Eq. (3)) and/or Fe³⁺ ions (Eq. (7)), which would precipitate on the NZVI surface (Eqs. (4) & (8)) and decrease the NZVI reactivity [10]. The precipitation process was evidenced by the variations of the Fe ion concentration during the corrosion process (Fig. S12a). Thus, the Al(OH)₃ coating shell could decrease the NZVI surface corrosion, leading to an extended longevity and long-term reactivity of NZVI. It was reported that the reactivity of NZVI could be protected in the air via encapsulation of NZVI particles inside poly(1-vinylpyrrolidone-co-vi-nylacetate) (PVV) vesicles [59]. However, the PVV vesicles would be ruptured immediately when they were placed in the aqueous solution, losing their ability of protecting the NZVI from aqueous corrosion.



The long-term leaching of Al ions was also assessed during the corrosion tests to evaluate the chemical stability of the Al(OH)₃ coating shell. Under different corrosion conditions, the concentration of dissolved Al ions varied from 0 to 10.3 µg/L for the pH range between 8.3 and 10.5 (Fig. S12b & S12c). As the total Al content in the suspension of NZVI@Al(OH)₃ at 1.0 wt% was equivalent to 1.0 mg/L, less than 1% of Al would be released from the coating surface of NZVI@Al(OH)₃ after a long-term exposure in the aqueous environment.

4. Conclusions

In this research, a thin Al(OH)₃ shell was successfully coated on the NZVI surface to simultaneously improve the suspension stability, reactivity and longevity of NZVI for potential environmental applications. The Al(OH)₃ coating layer changed the surface property of NZVI particles, such as ζ-potential, adsorption ability and corrosion resistance. As a result, the feasibility and effectiveness of NZVI@Al(OH)₃ particles were improved considerably for pollution control and environmental remediation. Moreover, coating a thin inorganic shell with multiple functions is shown as a promising approach to modify reactive nanoparticles. The facial coating process and the low dose of modification materials decrease the cost of synthesis and improve the effectiveness of the functional nanoparticles for environmental applications.

Acknowledgements

This research was supported by grants C7044-14G and T21-711/16R from the Research Grants Council (RGC) of the Hong Kong SAR government. The technical assistance of Mr. Keith C.H. Wong is greatly appreciated.

Appendix A. Supplementary data

Supplementary data associated with this article can be found, in the online version, at <https://doi.org/10.1016/j.apcatb.2017.12.077>.

References

- [1] H. Jabeen, V. Chandra, S. Jung, J.W. Lee, K.S. Kim, S.B. Kim, Enhanced Cr(VI) removal using iron nanoparticle decorated graphene, *Nanoscale* 3 (2011) 3583–3585.
- [2] C.J. Wei, X.-y. Li, Surface coating with Ca(OH)₂ for improvement of the transport of nanoscale zero-valent iron (nZVI) in porous media, *Water Sci. Technol.* 68 (2013) 2287–2293.
- [3] J. Tuček, R. Prucek, J. Kolařík, G. Zoppellaro, M. Petr, J. Filip, V.K. Sharma, R. Zbořil, Zero-valent iron nanoparticles reduce arsenites and arsenates to As(0) firmly embedded in core–shell superstructure: challenging strategy of arsenic treatment under anoxic conditions, *ACS Sustain. Chem. Eng.* (2017) 3027–3038.
- [4] M. Lawrinenko, Z. Wang, R. Horton, D. Mendivilso-Perez, E.A. Smith, T.E. Webster, D.A. Laird, J. van Leeuwen, Macroporous carbon supported zerovalent iron for remediation of trichloroethylene, *ACS Sustain. Chem. Eng.* (2016) 1586–1593.

[5] L. Tang, J. Tang, G. Zeng, G. Yang, X. Xie, Y. Zhou, Y. Pang, Y. Fang, J. Wang, W. Xiong, Rapid reductive degradation of aqueous p-nitrophenol using nanoscale zero-valent iron particles immobilized on mesoporous silica with enhanced anti-oxidation effect, *Appl. Surf. Sci.* 333 (2015) 220–228.

[6] T. Phenrat, N. Saleh, K. Sirk, R.D. Tilton, G.V. Lowry, Aggregation and sedimentation of aqueous nanoscale zerovalent iron dispersions, *Environ. Sci. Technol.* 41 (2007) 284–290.

[7] B. Schrick, B.W. Hydutsky, J.L. Blough, T.E. Mallouk, Delivery vehicles for zerovalent metal nanoparticles in soil and groundwater, *Chem. Mater.* 16 (2004) 2187–2193.

[8] Y. Zhang, Y. Li, J. Li, G. Sheng, Y. Zhang, X. Zheng, Enhanced Cr(VI) removal by using the mixture of pillared bentonite and zero-valent iron, *Chem. Eng. J.* 185–186 (185) (2012) 243–.

[9] T. Phenrat, N. Saleh, K. Sirk, H.-J. Kim, R. Tilton, G. Lowry, Stabilization of aqueous nanoscale zerovalent iron dispersions by anionic polyelectrolytes: adsorbed anionic polyelectrolyte layer properties and their effect on aggregation and sedimentation, *J. Nanopart. Res.* 10 (2008) 795–814.

[10] R.A. Crane, T.B. Scott, Nanoscale zero-valent iron: future prospects for an emerging water treatment technology, *J. Hazard. Mater.* 211–212 (211) (2012) 112–.

[11] H.-L. Lien, W.-X. Zhang, Nanoscale Pd/Fe bimetallic particles: catalytic effects of palladium on hydrodechlorination, *Appl. Catal. B: Environ.* 77 (2007) 110–116.

[12] J. Xu, X. Liu, G.V. Lowry, Z. Cao, H. Zhao, J.L. Zhou, X. Xu, Dechlorination mechanism of 2,4-dichlorophenol by magnetic MWNTs supported Pd/Fe nanohbrids: rapid adsorption, gradual dechlorination, and desorption of phenol, *ACS Appl. Mater. Interfaces* 8 (2016) 7333–7342.

[13] Y. Hwang, Y.-C. Lee, P.D. Mines, Y.S. Huh, H.R. Andersen, Nanoscale zero-valent iron (NZVI) synthesis in a Mg-aminoclay solution exhibits increased stability and reactivity for reductive decontamination, *Appl. Catal. B: Environ.* 147 (2014) 748–755.

[14] Y. Li, J. Li, Y. Zhang, Mechanism insights into enhanced Cr(VI) removal using nanoscale zerovalent iron supported on the pillared bentonite by macroscopic and spectroscopic studies, *J. Hazard. Mater.* 227–228 (227) (2012) 211–.

[15] Z. Liu, F. Zhang, S.K. Hoekman, T. Liu, C. Gai, N. Peng, Homogeneously dispersed zerovalent iron nanoparticles supported on hydrochar-derived porous carbon. Simple, in situ synthesis and use for de-chlorination of PCBs, *ACS Sustain. Chem. Eng.* (2016) 3261–3267.

[16] T. Phenrat, I. Kumloet, Electromagnetic induction of nanoscale zerovalent iron particles accelerates the degradation of chlorinated dense non-aqueous phase liquid: proof of concept, *Water Res.* 107 (2016) 19–28.

[17] S. Srirattana, K. Piaowan, G.V. Lowry, T. Phenrat, Electromagnetic induction of foam-based nanoscale zerovalent iron (NZVI) particles to thermally enhance non-aqueous phase liquid (NAPL) volatilization in unsaturated porous media: proof of concept, *Chemosphere* 183 (2017) 323–331.

[18] D. Krewski, R.A. Yokel, E. Nieboer, D. Borchelt, J. Cohen, J. Harry, S. Kacew, J. Lindsay, A.M. Mahfouz, V. Rondeau, Human health risk assessment for aluminum, aluminum oxide and aluminum hydroxide, *J. Toxicol. Env. Heal. B* 10 (2007) 1–269.

[19] M. Kosmulski, pH-dependent surface charging and points of zero charge II. Update, *J. Colloid Interface Sci.* 275 (2004) 214–224.

[20] M. Kosmulski, pH-dependent surface charging and points of zero charge: III. Update, *J. Colloid Interface Sci.* 298 (2006) 730–741.

[21] Y. Yan, W. Li, J. Yang, A. Zheng, F. Liu, X. Feng, D.L. Sparks, Mechanism of myoinositol hexakisphosphate sorption on amorphous aluminum hydroxide: spectroscopic evidence for rapid surface precipitation, *Environ. Sci. Technol.* 48 (2014) 6735–6742.

[22] T. Xu, J.G. Catalano, Impacts of surface site coordination on arsenate adsorption: macroscopic uptake and binding mechanisms on aluminum hydroxide surfaces, *Langmuir* 32 (2016) 13261–13269.

[23] X. Zhao, J. Wang, F. Wu, T. Wang, Y. Cai, Y. Shi, G. Jiang, Removal of fluoride from aqueous media by $\text{Fe}_3\text{O}_4@\text{Al(OH)}_3$ magnetic nanoparticles, *J. Hazard. Mater.* 173 (2010) 102–109.

[24] R. Ghosh Chaudhuri, S. Paria, Core/shell nanoparticles: classes, properties, synthesis mechanisms, characterization, and applications, *Chem. Rev.* 112 (2012) 2373–2433.

[25] Z.W. Seh, J. Kibsgaard, C.F. Dickens, I. Chorkendorff, J.K. Nørskov, T.F. Jaramillo, Combining theory and experiment in electrocatalysis: insights into materials design, *Science* 355 (2017).

[26] L. Lu, Z. Ai, J. Li, Z. Zheng, Q. Li, L. Zhang, Synthesis and characterization of $\text{Fe}-\text{Fe}_2\text{O}_3$ core-shell nanowires and nanonecklaces, *Cryst. Growth Des.* 7 (2007) 459–464.

[27] Z. Ai, Z. Gao, L. Zhang, W. He, J.J. Yin, Core–shell structure dependent reactivity of $\text{Fe}@\text{Fe}_2\text{O}_3$ nanowires on aerobic degradation of 4-chlorophenol, *Environ. Sci. Technol.* 47 (2013) 5344–5352.

[28] J. Chen, Z. Xiu, G.V. Lowry, P.J.J. Alvarez, Effect of natural organic matter on toxicity and reactivity of nano-scale zero-valent iron, *Water Res.* 45 (2011) 1995–2001.

[29] Y. Liu, S.A. Majetich, R.D. Tilton, D.S. Sholl, G.V. Lowry, TCE dechlorination rates pathways, and efficiency of nanoscale iron particles with different properties, *Environ. Sci. Technol.* 39 (2005) 1338–1345.

[30] D. Fan, G. O'Brien Johnson, P.G. Tratnyek, R.L. Johnson, Sulfidation of nano zerovalent iron (nZVI) for improved selectivity during in-situ chemical reduction (ISCR), *Environ. Sci. Technol.* 50 (2016) 9558–9565.

[31] S. Zhang, S. Gai, F. He, Y. Dai, P. Gao, L. Li, Y. Chen, P. Yang, Uniform $\text{Ni/SiO}_2@\text{Au}$ magnetic hollow microspheres: rational design and excellent catalytic performance in 4-nitrophenol reduction, *Nanoscale* 6 (2014) 7025–7032.

[32] H. Dong, Z. Jiang, J. Deng, C. Zhang, Y. Cheng, K. Hou, L. Zhang, L. Tang, G. Zeng, Physicochemical transformation of Fe/Ni bimetallic nanoparticles during aging in simulated groundwater and the consequent effect on contaminant removal, *Water Res.* 129 (2018) 51–57.

[33] J.T. Nurmi, P.G. Tratnyek, V. Sarathy, D.R. Baer, J.E. Amonette, K. Pecher, C. Wang, J.C. Linehan, D.W. Matson, R.L. Penn, M.D. Driessens, Characterization and properties of metallic iron nanoparticles: spectroscopy, electrochemistry, and kinetics, *Environ. Sci. Technol.* 39 (2005) 1221–1230.

[34] S. Bi, C. Wang, Q. Cao, C. Zhang, Studies on the mechanism of hydrolysis and polymerization of aluminum salts in aqueous solution: correlations between the core-links model and cage-like Keggin- Al_{13} model, *Coord. Chem. Rev.* 248 (2004) 441–455.

[35] P. Rengasamy, J. Oades, Interaction of monomeric and polymeric species of metal ions with clay surfaces. III. Aluminium (III) and chromium (III), *Soil Res.* 16 (1978) 53–66.

[36] H.-Z. Zhao, H.-Y. Wang, S. Dockko, Y. Zhang, The formation mechanism of Al_{13} and its purification with an ethanol-acetone fractional precipitation method, *Sep. Purif. Technol.* 81 (2011) 466–471.

[37] P. Mills, J.L. Sullivan, A study of the core level electrons in iron and its three oxides by means of X-ray photoelectron spectroscopy, *J. Phys. D: Appl. Phys.* 16 (1983) 723.

[38] G. Bhargava, I. Gouzman, C.M. Chun, T.A. Ramanarayanan, S.L. Bernasek, Characterization of the native surface thin film on pure polycrystalline iron: a high resolution XPS and TEM study, *Appl. Surf. Sci.* 253 (2007) 4322–4329.

[39] J. Ding, Q. Zhong, S. Zhang, Simultaneous removal of NO_x and SO_2 with H_2O_2 over Fe based catalysts at low temperature, *RSC Adv.* 4 (2014) 5394–5398.

[40] Q. Feng, T. Li, H. Teng, X. Zhang, Y. Zhang, C. Liu, J. Jin, Investigation on the corrosion and oxidation resistance of $\text{Ni}-\text{Al}_2\text{O}_3$ nano-composite coatings prepared by sediment co-deposition, *Surf. Coat. Technol.* 202 (2008) 4137–4144.

[41] A.P. Grosvenor, B.A. Kobe, M.C. Biesinger, N.S. McIntyre, Investigation of multiplet splitting of Fe 2p XPS spectra and bonding in iron compounds, *Surf. Interface Anal.* 36 (2004) 1564–1574.

[42] J.T. Klopprogge, L.V. Duong, B.J. Wood, R.L. Frost, XPS study of the major minerals in bauxite: gibbsite, bayerite and (pseudo-)boehmite, *J. Colloid Interface Sci.* 296 (2006) 572–576.

[43] H. Dong, Q. He, G. Zeng, L. Tang, C. Zhang, Y. Xie, Y. Zeng, F. Zhao, Y. Wu, Chromate removal by surface-modified nanoscale zero-valent iron: effect of different surface coatings and water chemistry, *J. Colloid Interface Sci.* 471 (2016) 7–13.

[44] H. Su, Z. Fang, P.E. Tsang, J. Fang, D. Zhao, Stabilisation of nanoscale zero-valent iron with biochar for enhanced transport and in-situ remediation of hexavalent chromium in soil, *Environ. Pollut.* 214 (2016) 94–100.

[45] J. Gregory, *Particles in Water: Properties and Processes*, CRC Press, 2005.

[46] G. Sposito, *The Environmental Chemistry of Aluminum*, Lewis Publishers, 1995.

[47] T. Phenrat, H.-J. Kim, F. Fagerlund, T. Illangasekare, R.D. Tilton, G.V. Lowry, Particle size distribution concentration, and magnetic attraction affect transport of polymer-modified Fe^0 nanoparticles in sand columns, *Environ. Sci. Technol.* 43 (2009) 5079–5085.

[48] Y. Liu, G.V. Lowry, Effect of particle age (Fe^0 content) and solution pH on NZVI reactivity: H_2 evolution and TCE dechlorination, *Environ. Sci. Technol.* 40 (2006) 6085–6090.

[49] K.-F. Chen, S. Li, W.-x. Zhang, Renewable hydrogen generation by bimetallic zero valent iron nanoparticles, *Chem. Eng. J.* 170 (2011) 562–567.

[50] S.R.C. Rajajayavel, S. Ghoshal, Enhanced reductive dechlorination of trichloroethylene by sulfidated nanoscale zerovalent iron, *Water Res.* 78 (2015) 144–153.

[51] J. Du, D. Che, X. Li, W. Guo, N. Ren, Factors affecting p-nitrophenol removal by microscale zero-valent iron coupling with weak magnetic field (WMF), *RSC Adv.* 7 (2017) 18231–18237.

[52] B. Lai, Y. Zhang, Z. Chen, P. Yang, Y. Zhou, J. Wang, Removal of p-nitrophenol (PNP) in aqueous solution by the micron-scale iron-copper (Fe/Cu) bimetallic particles, *Appl. Catal. B: Environ.* 144 (2014) 816–830.

[53] J. Tang, L. Tang, H. Feng, G. Zeng, H. Dong, C. Zhang, B. Huang, Y. Deng, J. Wang, Y. Zhou, pH-dependent degradation of p-nitrophenol by sulfidated nanoscale zerovalent iron under aerobic or anoxic conditions, *J. Hazard. Mater.* (2016) 581–590.

[54] S. Bae, S. Gim, H. Kim, K. Hanna, Effect of NaBH_4 on properties of nanoscale zerovalent iron and its catalytic activity for reduction of p-nitrophenol, *Appl. Catal. B: Environ.* 182 (2016) 541–549.

[55] Y. Mu, F. Jia, Z. Ai, L. Zhang, Iron oxide shell mediated environmental remediation properties of nano zero-valent iron, *Environmen. Sci.: Nano* 4 (2017) 27–45.

[56] S. Chen, Z.P. Xu, Q. Zhang, G.Q.M. Lu, Z.P. Hao, S. Liu, Studies on adsorption of phenol and 4-nitrophenol on MgAl-mixed oxide derived from MgAl-layered double hydroxide, *Sep. Purif. Technol.* 67 (2009) 194–200.

[57] X. Peng, X. Liu, Y. Zhou, B. Peng, L. Tang, L. Luo, B. Yao, Y. Deng, J. Tang, G. Zeng, New insights into the activity of a biochar supported nanoscale zerovalent iron composite and nanoscale zero valent iron under anaerobic or aerobic conditions, *RSC Adv.* 7 (2017) 8755–8761.

[58] T. Tosco, M. Petrangeli Papini, C. Cruz Viggi, R. Sethi, Nanoscale zerovalent iron particles for groundwater remediation: a review, *J. Clean. Prod.* 77 (2014) 10–21.

[59] D. Shi, X. Zhang, J. Wang, G. Fan, Highly reactive and stable nanoscale zerovalent iron prepared within vesicles and its high-performance removal of water pollutants, *Appl. Catal. B: Environ.* 221 (2018) 610–617.